Mechanical Systems and Signal Processing 161 (2021) 107987

Contents lists available at ScienceDirect

Mechanical Systems and Signal Processing

journal homepage: www.elsevier.com/locate/ymssp

Chatter formation during milling due to stochastic noise-induced resonance

Henrik T Sykora *, David Hajdu, Zoltan Dombovari, Daniel Bachrathy

MTA-BME Lendület Machine Tool Vibration Research Group, Department of Applied Mechanics, Budapest University of Technology and Economics, Budapest, Hungary

ARTICLE INFO

Communicated by Giovanni Totis

Keywords:
Milling
Stochastic delay differential equation
Stochastic cutting force
Machine tool vibrations
Time-delay
Chatter detection
Stationary second moment

ABSTRACT

In this paper, the stochastic dynamical model of a single-degree-of-freedom milling operation is formulated, where a Gaussian white noise process models the high-frequency variation in the cutting force. With the help of this stochastic model, it is shown, that large-amplitude stable vibrations can occur near the critical machining parameters, due to stochastic noise-induced resonance. During the analysis, the second moment stability and stationary first and second moment behavior of the periodic stochastic delay differential equation (SDDE) describing the milling operation are investigated. The behavior of these quantities are then compared to the evolution of the so-called "chatter peak" in the Fourier-spectrum of the vibrations, that is used to experimentally determine the presence of chatter, in the stable machining parameter domain. Furthermore, it is discussed, how the statistical properties of the resonant vibrations can be used to predict the stability boundary and the formulation of chatter, while the machining parameters are kept in the safe region. The theoretical calculations are supported by experiments performed on a single-degree-of-freedom system.

1. Introduction

Machine tool industry is a competitive sector which highly utilizes new technological developments and innovations. Newest machining centers are dynamically stiff and robust designs intended to operate at high speeds and at large material removal rates. However, very often these capabilities of the machines are not accessible due to the arising undesired self-excited vibrations. These large-amplitude vibrations (also called *chatter*) cause unacceptable surface finish, increase tool wear, and possibly damage machining components. Due to the flexibility of the tools, this phenomenon often occurs during roughing operations for larger material removal rates, and the suppression of these vibrations is a challenge even for the machining experts. The high modeling complexity and large computational effort required for simulations also make it very complicated to analyze the underlying nature of chatter vibrations.

During a cutting operation the geometry of the chip is affected by the relative vibration between the tool and the workpiece. The chip thickness is affected by the subsequent cuts, namely the present cut and the past cut, and it makes the cutting force dependent on the past motion of the tool (and workpiece). This is the regenerative effect, which is mathematically modeled by delay differential equations (DDE). The first promising mathematical models dealing with the evolution of chatter were published by Tobias [53] and

* Corresponding author at: Budapest University of Technology and Economics, Department of Applied Mechanics, MTA-BME Lendület Machine Tool Vibration Research Group, H-1111 Budapest, Hungary.

E-mail addresses: sykora@mm.bme.hu (H.T. Sykora), hajdu@mm.bme.hu (D. Hajdu), dombovari@mm.bme.hu (Z. Dombovari), bachrathy@mm.bme.hu (D. Bachrathy).

https://doi.org/10.1016/j.ymssp.2021.107987
Received 30 December 2020; Received in revised form 19 March 2021; Accepted 19 April 2021
Available online 4 May 2021

Tlusty [52], who introduced the time-delay and the regenerative effect in the mechanical models. This laid down the fundamentals of machine tool vibration research, which still interests engineers and applied mathematicians.

In the last few decades, several numerical methods have been proposed to efficiently predict the appearance of unstable vibrations. These stability properties (stable or unstable) are graphically represented by the so-called stability lobe diagrams, which plot the stable parameter regions as a function of the spindle speed (or sometimes other machining parameters). Numerical methods, such as the *multi-frequency solution* [11], the *semidiscretization method* [24], or the *spectral element method* [29], to mention a few, are developed for deterministic systems, where parameters are assumed to be fixed and free of noise. The predictions obtained for deterministic systems by such methods often fail to accurately predict the real stability boundaries due to modeling uncertainties and simplifications. In order to take into account uncertainties, new methods have been proposed, where some system parameters are assumed to be not perfectly known, but still static in time. For example, statistical methods, such as the *Polynomial Chaos-Kriging approach* [55] considers uncertainties in the modal parameters and cutting coefficients and results in statistical diagrams including the probability of instability. In the meantime, robust methods, such as the *extended multi-frequency solution with structured singular values* [21] consider bounded uncertainties without statistical distributions, providing guaranteed safe margins of stability. These methods can improve the reliability of predictions, but there might be limitations in the applications, such as the high computational effort, modeling difficulties, large number of parameters and unknown statistical distributions, see the works [55,21] and the references therein.

Methods used for the prediction of stability lobe diagrams (SLDs) are called *out-of-process* solutions (or sometimes off-line methods), since the limit machining parameters are determined prior to the cutting process. As opposed to this, *in-process* techniques are often called *chatter detection* methods (or on-line methods), because the recognition of unstable vibrations are done during the machining [44]. Furthermore, due to the various applications, different perspectives on classification exist [44,47]. Detection methods are often based on the recorded signals captured by different sensors, on the surface quality of the machined workpiece, or on other indicators, which show the appearance of chatter marks. Based on the physical contact between the machine and sensors, direct and indirect methods can be distinguished [47]. For example, dynamometers, strain gauges, thermal sensors, or accelerometers are classified as direct instruments, while optical and sonic sensors are contact-less, and are therefore called indirect.

Classification can also be done based on the evaluation process of the recorded signals typically captured by dynamometers, accelerometers or microphones. Some techniques apply to the measured signals in time domain considering the properties of the time-periodic system, for example, [35,26] presented identification methods, which compute the dominant Floquet multipliers of the system, in [34] the Q-factor is used to approximate the closeness of the stability boundaries, or use recurrence quantification analysis [46] to identify chatter vibrations. Other methods include the analysis of the statistical properties of the measured signals, e.g., the probability density function of the cutting force [17], or the RMS of the measured velocity signals [7] are considered to determine the stability of the machining process. There are works, where data science and machine learning techniques are used to capture the presence of chatter, e.g., the topology of the point cloud generated by the measured vibration signals [25] or a support vector machine is used to classify the vibrations [56]. Most of the other methods rather calculate the frequency spectra of the captured signals and examine it for the chatter frequencies. Audio signals are used by [14,3], force signals are applied by [31] for chatter detection and mitigation, and the calculation of a chatter indicator function is presented by [27] based on the power spectra of signals captured by a multi-sensor system. In [33,30] the spectral entropy computed from the power spectra is used to indentify chatter vibrations. For a detailed review on chatter detection methods and for a more complete list of techniques, see [44].

The main drawback of on-line techniques is that these methods are usually capable to detect chatter only when it is already developed, which means that only posterior actions can done. There is a high potential in methods, which can detect chatter as soon as possible, when it just starts to evolve (or even before), as pointed out by many researchers [44]. For this purpose, great efforts were made to utilize automatic chatter detection during machining, however, the evaluation in most of the practical cases is still based on empirical expertise [4,18,27].

Beside the self-excited vibrations, there is an another source of vibration which affects the cutting conditions. The so-called forced vibrations are the results of the non-state-dependent time-varying component of the cutting force. This occurs due to the changing size and shape of the chip, but also can be caused by high-frequency processes [57] such as chip formation and segmentation [20,40], shockwaves, material grain direction and local inhomogeneities in the material properties [41–43], shear plane oscillation [8], rough surface of the workpiece [32], friction, etc. However, similarly to the uncertainties, these variations are usually not considered in the constant parameters of the force characteristics describing the relationship between the cutting force and the chip size, although these cutting force fluctuations may significantly influence the behavior of these systems. During the measurement of the cutting force, these high-frequency cutting force variations are usually attributed to the quality of the measurement, however, these variations are orders of magnitude larger than being explained by measurement noise. These high-speed phenomena are very complex processes, and there are ways to model these variances in the cutting force, e.g., using sophisticated finite element method [9,13] to compute the chip formation or using a simplified shear zone model [2]. However, these approaches require a large number and hardly measurable parameters, are computationally expensive and difficult to evaluate. Furthermore, they do not provide an efficient tool to analyze how these high-frequency fluctuations in the cutting force influence the stability of the cutting process.

Recently, stochastic processes are introduced [19] as a concise way of modeling these variations in the cutting processes. It is observed that the noise can be represented by multiplicative model, and additionally, an equivalent white noise process is proposed and fitted on the measured power spectra of the cutting force. This approach allowed to show that the fluctuations do not significantly influence the stability properties of turning processes [19,49], however, it causes large amplitude vibrations near the stability boundaries. These vibrations are potentially falsely identified as chatter, or it can even cause a transition to chatter in the unsafe (bistable) zones near the stability borders [16,37]. Due to such phenomena, the evaluation of experimental data is often challenging, and even experts cannot always distinguish the real unstable and stable operations in practice (these are often marked as *marginal*).

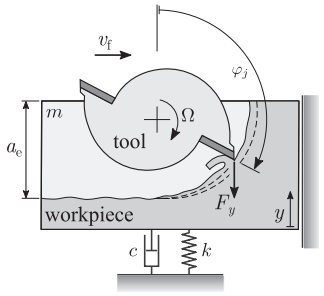

Fig. 1. Single-degree-of-freedom mechanical model of milling with axial depth of cut a_p.

This paper aims to discuss how milling operation are affected by high-frequency cutting force fluctuations and give a mathematically well-established derivation for its stochastic model (Section 2). Opposed to the deterministic models, this proposed so-called *stochastic noise-induced resonance* (Appendix A) can explain the unexpected appearance of chatter vibrations under stable machining conditions [16], and can even be used for chatter detection by predicting the margins of stability (Section 3). It is shown that if the noise-induced resonance is considered during machining, then the uncertainty of chatter detection can be explained and accounted for, allowing to create more reliable expert systems to classify cutting processes as stable or unstable. Experimental validations are also presented, which show good qualitative agreement with numerical simulations. A detailed summary and a conclusion are given at the end of the paper in Section 4.

2. Stochastic model of milling

In this section, the stochastic model of a single-degree-of-freedom milling layout is constructed by considering the high-frequency variations of the cutting force as a white noise excitation. Next, the behavior of the periodic stochastic delay differential equation (periodic SDDE) describing the relative vibrations of the milling tool and the workpiece is investigated; namely, its first and second-moment stability, steady-state first and second-moment behavior, and the Fourier spectrum of the simulated motion are analyzed. Note that the concepts of first and second moments are used here in the statistical sense; namely, they refer to the time-dependent mean and mean square of the process describing the milling.

2.1. Deterministic model of milling

Accurate prediction of machining relies on the precise measurement of dynamical parameters and cutting force characteristics for the used machine-tool-workpiece system and the cutter-workpiece engagement. This section serves as an introduction to present the basics of the derivation of the stochastic modeling of milling operations. Here a simple model is used, which allows focusing on the effect of the stochastic cutting force on the dynamics of the milling operations. The simplified dynamical model [26] is shown in Fig. 1, where the tool is assumed to be completely rigid while the workpiece vibrates perpendicular to the feed direction (similarly to a plate under a finishing operation).

The governing deterministic equation of motion is

$$m\ddot{y}(t) + c\dot{y}(t) + ky(t) = -F_y(t), \tag{1}$$

where $F_y(t)$ denotes the cutting force component in the direction of the displacement y of the workpiece, while m, c and k are the modal mass, damping and stiffness, respectively. The cutting force component in the direction of the feed is omitted due to the geometric constraint. The cutting force characteristics is assumed to be linear [1], which gives the force for the straight fluted tool:

$$F_y(t) = a_p \sum_{j=1}^{Z} \big(-K_t \sin\varphi_j(t) + K_r \cos\varphi_j(t) \big) g_j(t) h_j(t), \tag{2}$$

where a_p is the axial depth of cut, K_t and K_r are the tangential and radial cutting force coefficients, respectively, and φ_j is the angular position of tooth j. The chip thickness $h_j(t)$ at tooth j can be approximated as

$$h_j(t) \approx f_Z \sin\varphi_j(t) + (y(t) - y(t - T_Z))\cos\varphi_j(t), \tag{3}$$

where $f_Z = v_f T_Z$ is the feed per tooth in the feed direction and $T_Z = 2\pi/(Z\Omega)$ is tooth passing period, while Z is the number of the cutting edges. Here $\Omega = 2\pi n/60$ is the spindle speed in rad/s and n is the spindle speed in rpm. Since the two quantities differ only in a constant multiplier, their use is interchangeable throughout this paper. In this simple model the regenerative time delay is $\tau \equiv T_Z$. The screen function $g_j(t)$ shows whether the j-th edge cuts into the material and can be given as

$$g_j(t) = \begin{cases} 1, & \text{if } \varphi_{\text{en}} < \big(\varphi_j(t) \bmod 2\pi\big) < \varphi_{\text{ex}}, \\ 0, & \text{otherwise}, \end{cases} \tag{4}$$

where φ_{en} denotes the angular position where the tooth enters into the material, while φ_{ex} is where the tooth exits the material.

2.2. Stochastic extension of the model of milling

To account the high-frequency phenomena during the cutting process a multiplicative noise component is added to the deterministic model [50,19]. The resulting stochastic cutting force coefficients are

$$K_{\text{t},t} = K_{\text{t}}(1 + \sigma_0 \Gamma_t) \text{ and } K_{\text{r},t} = K_{\text{r}}(1 + \sigma_0 \Gamma_t), \tag{5}$$

where Γ_t is the Gaussian white noise approximation of the fluctuations in the cutting force, while σ_0 corresponds to the intensity of this white noise. The stochastic process Γ_t is often referred to as the Langevin force that is independent of the position and the velocity of the tool, its previous values $\Gamma_{\widehat{t}}$, $\widehat{t} < t$, and has constant power spectra (hence the name "white noise"). Similarly to [5], the stochastic and deterministic processes are distinguished by the following notation: the subscript t (e.g., $\mathbf{x}_t$ or Γ_t) refers to the time dependence of a stochastic process, while (t) in parenthesis (e.g., $\varphi_j(t)$) indicates a time-dependent deterministic process.

The cutting force (2) with the introduced stochastic coefficients reduces to

$$F_{y,t} = a_{\text{p}} \sum_{j=1}^{Z} \big(-K_{\text{t}} \sin\varphi_j(t) + K_{\text{r}} \cos\varphi_j(t) \big) g_j(t) h_{j,t} + a_{\text{p}} \sigma_0 \sum_{j=1}^{Z} \big(-K_{\text{t}} \sin\varphi_j(t) + K_{\text{r}} \cos\varphi_j(t) \big) g_j(t) h_{j,t} \Gamma_{j,t}. \tag{6}$$

Note that the chip thickness $h_{j,t}$ also becomes stochastic. Additionally, there are multiple independent stochastic noises $\Gamma_{j,t}$ present in the cutting force (6) corresponding to each cutting tooth. The SDDE describing the dynamics of the milling process is

$$m\ddot{y}_t + c\dot{y}_t + k y_t = -a_{\text{p}} \sum_{j=1}^{Z} \big(-K_{\text{t}} \sin\varphi_j(t) + K_{\text{r}} \cos\varphi_j(t) \big) g_j(t) h_{j,t} - a_{\text{p}} \sigma_0 \sum_{j=1}^{Z} \big(-K_{\text{t}} \sin\varphi_j(t) + K_{\text{r}} \cos\varphi_j(t) \big) g_j(t) h_{j,t} \Gamma_{j,t}. \tag{7}$$

The solution of (7) with the stochastic cutting force defined in (6) can be partitioned into a dimensionless periodic deterministic $x_{\text{p}}(t)$ and into a dimensionless stochastic x_t component as

$$y_t = f_{\text{Z}}\big(x_{\text{p}}(t) + x_t\big), \tag{8}$$

where $x_{\text{p}}(t) = x_{\text{p}}(t + T_{\text{Z}})$ and $\mathbb{E}(x_t) = 0$, where $\mathbb{E}(\cdot)$ denotes the expectation value. Furthermore, in order to have a better-conditioned dynamical system for the numerical simulations, one can introduce the dimensionless time $\widehat{t} = \omega_{\text{n}} t$, where $\omega_{\text{n}}^2 = k/m$ is the undamped natural frequency of the single-degree-of-freedom system and $\zeta = c/(2m\omega_{\text{n}})$ is the damping ratio. Substituting (3) and (8) into (7) leads to the dimensionless equation of motion

$$\Big(x_{\text{p}}''(\widehat{t}) + 2\zeta x_{\text{p}}'(\widehat{t}) + x_{\text{p}}(\widehat{t})\Big) + \big(x_{\widehat{t}}'' + 2\zeta x_{\widehat{t}}' + x_{\widehat{t}}\big) = -H\big(G_{\text{s}}(\widehat{t}) + G_{\text{c}}(\widehat{t})(x_{\widehat{t}} + x_{\widehat{t}-\widehat{\tau}})\big) - \sum_{j=1}^{Z} \widehat{\sigma} H\big(G_{\text{s},j}(\widehat{t}) + G_{\text{c},j}(\widehat{t})(x_{\widehat{t}} + x_{\widehat{t}-\widehat{\tau}})\big)\Gamma_{j,t}. \tag{9}$$

Here $\square'$ denotes the differentiation with respect to the dimensionless time $\widehat{t}$, $\widehat{T}_{\text{Z}} = 2\pi/(Z\widehat{\Omega}), \widehat{\tau} := \widehat{T}_{\text{Z}}, \widehat{\Omega} = \Omega/\omega_{\text{n}}, H = a_{\text{p}} K_{\text{t}}/\big(m\omega_{\text{n}}^2\big)$ and $\widehat{\sigma} = \sqrt{\omega_{\text{n}}}\sigma_0$ due to the rescaling properties of the Langevin force [39]. The deterministic periodic coefficients can be expressed as $G_{\text{c}}(\widehat{t}) = \sum_{j=1}^{Z} G_{\text{c}j}(\widehat{t})$ and $G_{\text{s}}(\widehat{t}) = \sum_{j=1}^{Z} G_{\text{s}j}(\widehat{t})$, where

$$G_{\text{c},j}(\widehat{t}) = \big(-\sin\varphi_j(\widehat{t}) + r\cos\varphi_j(\widehat{t})\big)\cos\varphi_j(\widehat{t}) g_j(\widehat{t}), \tag{10}$$

$$G_{\text{s},j}(\widehat{t}) = \big(-\sin\varphi_j(\widehat{t}) + r\cos\varphi_j(\widehat{t})\big)\sin\varphi_j(\widehat{t}) g_j(\widehat{t}), \tag{11}$$

with $r = K_{\text{r}}/K_{\text{t}}$. Assuming constant spindle speed, the angular positions $\varphi_j(\widehat{t})$ can be written as

$$\varphi_j(\widehat{t}) = \widehat{\Omega}\widehat{t} - (j-1)\frac{2\pi}{Z}. \tag{12}$$

The differential equation for the deterministic periodic solution $x_{\text{p}}(\widehat{t})$ can be obtained by taking the expectation value of Eq. (9). The first-order form of the resulting equation is

$$\mathbf{x}_{\text{p}}'(\widehat{t}) = \mathbf{A}_0 \mathbf{x}_{\text{p}}(\widehat{t}) + \mathbf{c}(\widehat{t}), \tag{13}$$

where

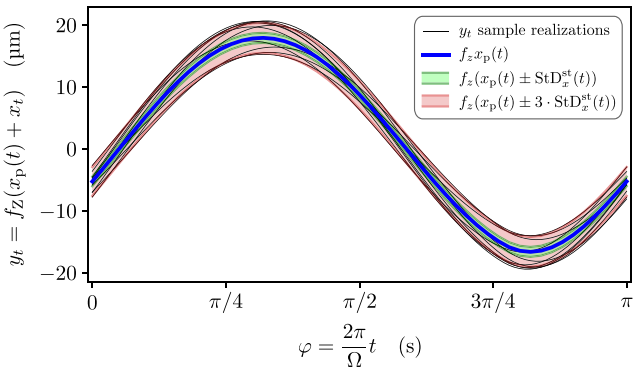

Fig. 2. Example trajectories (10 realizations) for the stationary vibrations y_t, for the steady-state deterministic solution $x_p(t)$ (first moment of y_t) and the 1 and 3 standard deviation (StD) zones.

$$\mathbf{x}_p(\hat{t}) = \begin{pmatrix} x_p(\hat{t}) \\ x_p'(\hat{t}) \end{pmatrix}, \qquad \mathbf{A}_0 = \begin{pmatrix} 0 & 1 \\ -1 & -2\zeta \end{pmatrix}, \qquad \mathbf{c}(\hat{t}) = \begin{pmatrix} 0 \\ -HG_s(\hat{t}) \end{pmatrix}. \tag{14}$$

Subtracting (13) from (9) leads to the equation of motion for the stochastic perturbation $x_{\hat{t}}$, that can be given in the first-order incremental form

$$\mathrm{d}\mathbf{x}_{\hat{t}} = \left(\mathbf{A}(\hat{t})\mathbf{x}_{\hat{t}} + \mathbf{B}(\hat{t})\mathbf{x}_{\hat{t}-\hat{\tau}}\right)\mathrm{d}\hat{t} + \sum_{j=1}^{Z}\left(\boldsymbol{\alpha}_j(\hat{t})\mathbf{x}_{\hat{t}} + \boldsymbol{\beta}_j(\hat{t})\mathbf{x}_{\hat{t}-\hat{\tau}} + \boldsymbol{\sigma}_j(\hat{t})\right)\mathrm{d}W_{j,\hat{t}}, \tag{15}$$

where

$$\begin{aligned} &\mathbf{x}_{\hat{t}} = \begin{pmatrix} x_{\hat{t}} \\ x_{\hat{t}}' \end{pmatrix}, \qquad \mathbf{A}(\hat{t}) = \mathbf{A}_0 + \begin{pmatrix} 0 & 0 \\ -HG_c(\hat{t}) & 0 \end{pmatrix}, \qquad \mathbf{B}(\hat{t}) = \begin{pmatrix} 0 & 0 \\ HG_c(\hat{t}) & 0 \end{pmatrix}, \\ &\boldsymbol{\alpha}_j(\hat{t}) = \begin{pmatrix} 0 & 0 \\ -\hat{\sigma}HG_{c,j}(\hat{t}) & 0 \end{pmatrix}, \ \boldsymbol{\beta}_j(\hat{t}) = \begin{pmatrix} 0 & 0 \\ \hat{\sigma}HG_{c,j}(\hat{t}) & 0 \end{pmatrix}, \ \boldsymbol{\sigma}_j(\hat{t}) = \begin{pmatrix} 0 \\ -\hat{\sigma}HG_{s,j}(\hat{t}) \end{pmatrix}. \end{aligned} \tag{16}$$

In (16) the coefficients are partitioned according to the form given in [49]. The process $W_{j,\hat{t}}$ denotes the Wiener process that is obtained by integrating the Langevin force, i.e.,

$$W_{j,\hat{t}_2} - W_{j,\hat{t}_1} := \int_{\hat{t}_1}^{\hat{t}_2} \Gamma_{j,s}\mathrm{d}s \text{ and } \mathrm{d}W_t := \int_{\hat{t}}^{\hat{t}+\mathrm{d}\hat{t}} \Gamma_{j,s}\mathrm{d}s, \tag{17}$$

where $\mathrm{d}W_t$ is referred to as the Wiener increment. Note that the model leads to additive and multiplicative noise for both x_t and $x_{t-\tau}$, which can potentially cause a change in the stability properties. As an abuse of notation, from this point the dimensionless time variable $\hat{t}$ is denoted with t.

To investigate the behavior of milling subjected to stochastic cutting force excitation, one needs (13) to determine the stationary deterministic periodic first moment $x_p(t)$, while (15) allows the first and second moment stability investigation of this periodic solution and the calculation of the stationary periodic second moment of the process $x_{\hat{t}}$.

The deterministic periodic first moment $x_p(t)$ can be utilized to qualify the steady-state mean behavior or average behavior of system (7). For this purpose the peak-to-peak (P2P) amplitude of $x_p(t)$ is used, which is defined as

$$\mathrm{P2P}(x_p) = \left(\max_{t\in\left[-\hat{T}_Z,0\right]} x_p(t)\right) - \left(\min_{t\in\left[-\hat{T}_Z,0\right]} x_p(t)\right). \tag{18}$$

To investigate the noise-induced resonance near the stability borders described by the proposed stochastic cutting force, the maximum and the time average of the steady-state standard deviation is used, namely,

$$\max_{t\in\left[-\hat{T}_Z,0\right]} \mathrm{StD}_x^{st}(t) \quad \text{and} \quad \operatorname{mean}_{t\in\left[-\hat{T}_Z,0\right]} \mathrm{StD}_x^{st}(t), \tag{19}$$

respectively, where

$$\mathrm{StD}_x^{st}(s) = \lim_{k\to\infty} \mathrm{StD}\left(x_{\hat{kT}_Z+s}\right) \quad \text{where} \quad s \in \left[-\hat{T}_Z, 0\right]. \tag{20}$$

In Fig. 2 an illustration is given for the steady-state periodic solution x_p, realizations for y_t and how the periodic steady-state

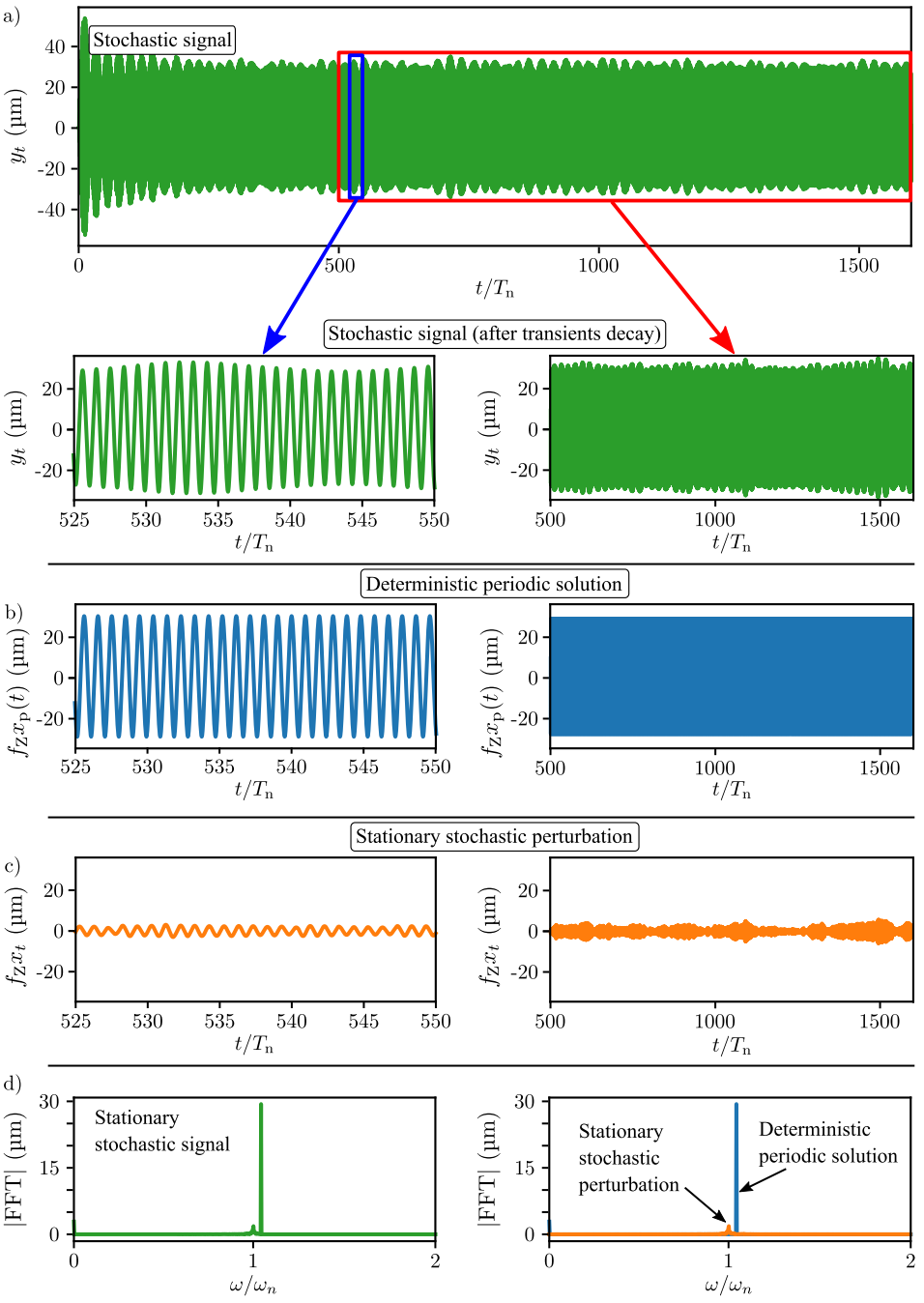

Fig. 3. Draft of the trajectory decomposition of the stationary trajectories: a) the entire stochastic signal, b) deterministic periodic component, c) stationary stochastic component. In panels d) the Fourier spectrum of the stationary trajectory and the decomposed trajectories can be seen.

standard deviation $\mathrm{StD}_x^{\mathrm{st}}$ can be interpreted.

These indicators along with the stability properties can be directly computed with the stochastic semidiscretization method by supplying the coefficient matrices defined in (13)–(14) and (15)–(16) to the Julia package *StochasticSemidiscretizationMethod.jl* [48]. This package is a high-performance and efficient implementation of the stochastic semidiscretization [49,51] of linear periodic stochastic delay differential equations. During stochastic semidiscretization the stochastic differential equation with periodic coefficients is approximated with a discrete stochastic map for which the first and second moment mappings are calculated. Thus, the package is capable of approximating the first and second moment stability and steady-state first and second moments of linear periodic stochastic systems, where the first moment is used to characterize the mean behavior, while the second moment describes the mean square dynamics that contains the stochastic effects. To calculate the $\mathrm{P2P}(\boldsymbol{x}_{\mathrm{p}}(t))$ values defined in (18) the discretized periodic steady state

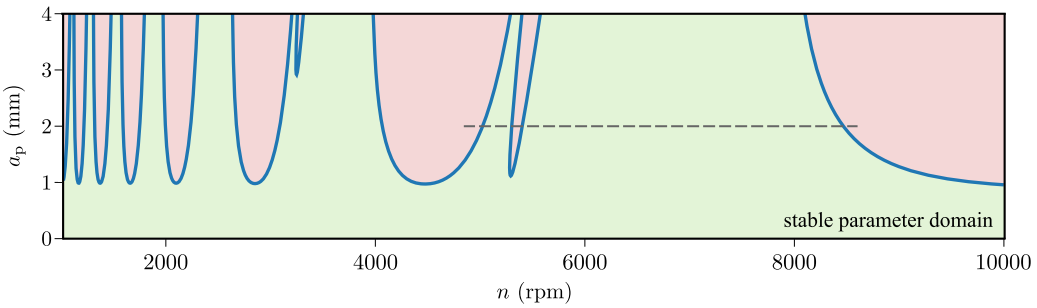

Fig. 4. First and second moment stability chart of a milling operation. The difference between the two charts are within the linewidth. The green region denotes the stable parameter region, while the light red domain denotes the parameters where chatter occurs. The black dashed line denotes the value range investigated in Fig. 6.

first moment of (13) is used, while to determine the maximum and the time average of the standard deviation in (19) the discretized periodic steady-state second moment of (15) is utilized.

Next, to allow the analysis of the Fourier spectra of the vibrations x_t (as it is a typical method during chatter detection during measurements), the Eq. (9) is utilized to numerically calculate realizations of the milling process. Then, after the transient vibrations decayed (which is assumed to happen after 5000 natural period $T_n := 2\pi/\omega_n$), the steady-state section of the trajectory is decomposed into the deterministic periodic solution $x_p(t)$ and into the stochastic perturbation x_t. The deterministic periodic solution $f_Z x_p(t)$ is obtained by periodically averaging the simulated result y_t with the tooth passing period T_Z, while the stochastic perturbation $f_Z x_t$ was acquired by subtraction: $f_Z x_t = y_t - f_Z x_p(t)$. Next, to investigate the noise-induced resonance, the Fourier transform of the stochastic perturbation x_t is computed in the stationary section, namely

$$\ell_{\text{peak}} = \max_{\omega} |\text{FFT}\{x_t\}(\omega)|. \tag{21}$$

The draft of this decomposition is illustrated in Fig. 3. In Fig. 3(a) the original stationary trajectory is shown, while b) and c) show the periodic deterministic and the stationary stochastic perturbation components, respectively. Along with the trajectories the magnitude of the Fourier transform of the stationary trajectory y_t and the decomposed trajectories $f_Z x_p(t)$ and $f_Z x_t$ are shown in Fig. 3d). In the Fourier transform of y_t peaks can be observed at the excitation frequency and its higher harmonics, and at the chatter frequency, which is typically close to the natural frequency ω_n. When analyzing the Fourier transform of the decomposed vibrations, the harmonics at the excitation frequencies appear only in the deterministic periodic component. However, in the Fourier transform of the stochastic component x_t of a trajectory a well-defined peak can be observed close to the natural frequency ω_n, while there is no peak at the excitation frequencies. This peak is usually referred to as the "chatter-peak" of the mechanical system and based on the model presented in this paper, its growth is attributed to the noise-induced resonance.

To investigate the effect of machining parameters on the indicators described in (18), (19) and (21) a numerical analysis was conducted. For this analysis of the stochastic model of milling, some numerical parameters were chosen based on [26]. The modal parameters of the test rig were identified through impact modal tests; the modal mass, damping and natural frequency are $m = 2.701$ kg, $\zeta = 0.71\%$ and $\omega_n = 259.96$ Hz, respectively. The milling operation is assumed to be conducted with a straight-edged two-fluted tool ($Z = 2$) with diameter $D = 16$ mm and with a feed per tooth $f_Z = 0.1$ mm/tooth. In this case study down-milling operation is considered with radial immersion $a_e = 2$ mm, which results in $\varphi_{en} = 138.6°$ and $\varphi_{ex} = 180°$.

Finally, the cutting force coefficients K_t and K_r were determined through a series of cutting tests, that were performed on an AL2024-T351 workpiece clamped onto a Kistler 9129AA dynamometer. The measurements were conducted with full immersion milling with axial depths of cut of $a_p = 1$ mm and 2 mm, and for feed per tooth values $f_Z = 0.02$ mm and 0.2 mm with $\Delta f_Z = 0.02$ mm steps. The spindle speed was $n = 8000$ rpm. Based on [12] and Section 2.8.1 of [2] the cutting force coefficients K_t and K_r were fitted on the time-average of the cutting force signal measured on 50 mm long sections. The measured radial and tangential cutting force coefficients are $K_r = 0.175 \cdot 10^9$ N/m^2 and $K_t = 1.095 \cdot 10^9$ N/m^2, respectively, resulting in $r = 0.16$, as defined in (10). Based on the measurement results in [19,50], the intensity of the noise component in the cutting force is assumed to be as small as $\sigma_0 = 0.5\,\%$. During semidiscretization the period resolution $p = 50$ and the Lagrange polynomial order $q = 3$ was chosen, while the trajectories for the analysis of the Fourier spectra were calculated using the stabilized SROCK [45] method (through the *StochasticDelayDiffEq.jl* package) with time step $\delta t = 10^{-3} \cdot 2\pi/\omega_n \approx 3.847 \cdot 10^{-6}$ s.

Since the noise is a very low intensity component of the cutting force, it has no significant effect on the stability of milling determined based on the deterministic model, similarly to turning operations as detailed in [19,49]. Thus both the semi-discretized first and second moment stability, computed with the package *StochasticSemidiscretizationMethod.jl* can be used to determine stability on the parameter region $a_p \in [0, 4\text{ mm}]$ and $n \in [1000\text{ rpm}, 10000\text{ rpm}]$, as shown in Fig. 4. In order to analyze the P2P of the steady-state periodic first moment, $x_p(t)$ is approximated with the help of the fixed-point of the first moment map generated from (13). Similarly, to compute the maximum and mean values of the steady-state second moment, it is approximated with the help of the fixed point of the second moment map constructed from (15). During the calculations the axial depth of cut was fixed for $a_p = 2$ mm and the analysis was performed on spindle speed interval $n \in [4800\text{ rpm}, 8600\text{ rpm}]$.

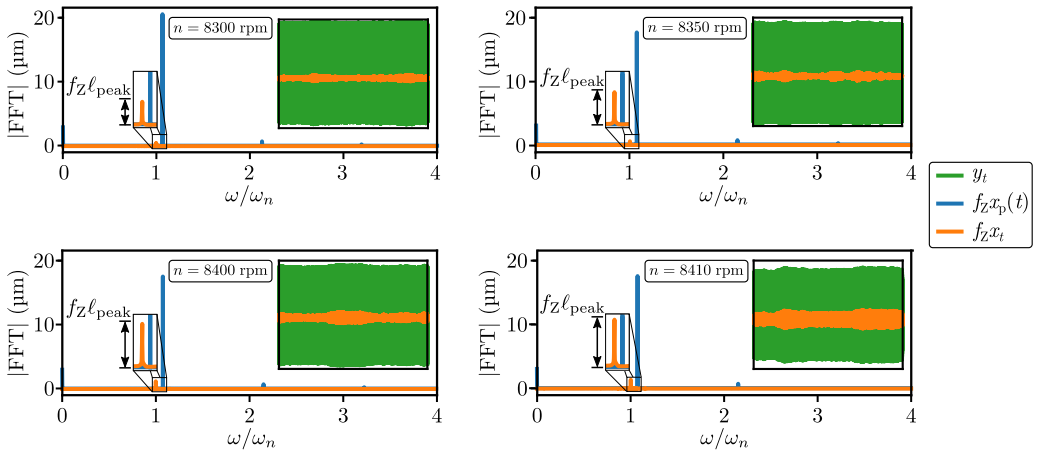

Fig. 5. Examples of the Fourier transforms of the decomposed stationary trajectories. The blue peaks denote the Fourier transforms of the periodic deterministic solution, while the orange peaks denotes the Fourier transforms of the noise perturbation. For each Fourier transforms the draft of the simulated trajectory is given in green, while the orange trajectory denotes the separated noise perturbation component of the trajectory.

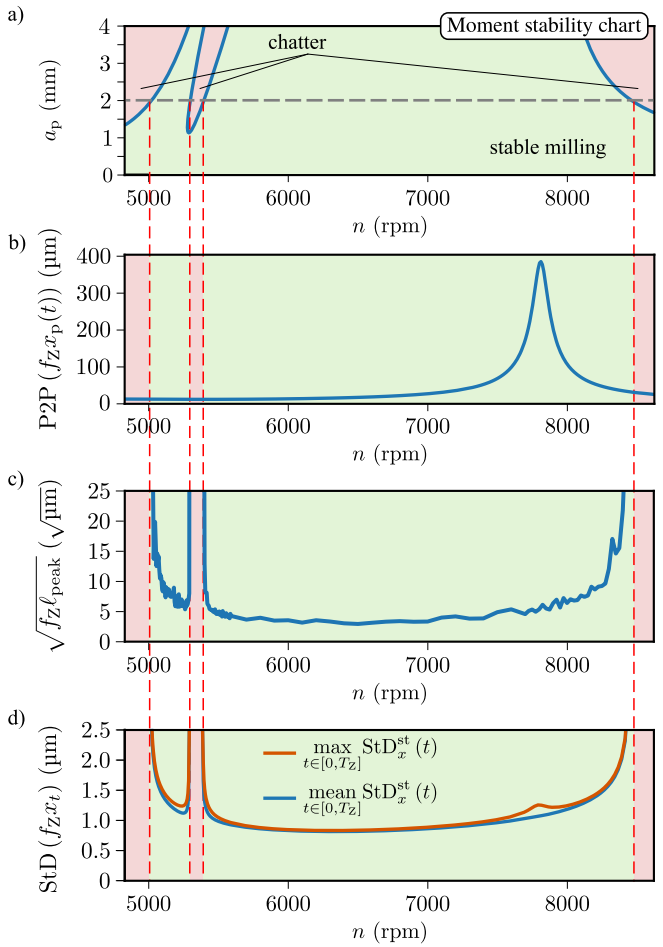

Fig. 6. Stability analysis of a milling operation. Panel a) shows the moment stability chart, where the shaded area denotes the stable parameters, panel b) shows the peak-to-peak (P2P) values of the steady-state deterministic periodic solution $f_Z x_p(t)$, panel c) shows the standard deviation (StD) of the stochastic perturbation $f_Z x_t$, while panel d) illustrates the behavior of the peak height ℓ_{peak} of the Fourier spectrum of the stochastic perturbation x_t.

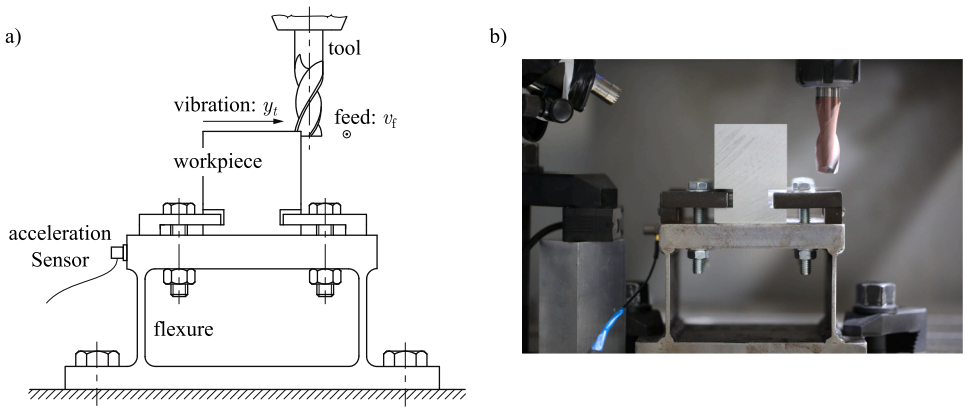

Fig. 7. Experimental setup to measure the single-degree-of-freedom vibrations during milling. Panel a) shows the schematic figure, while panel b) presents the experimental setup, as presented in [26].

First, the behavior of the FRF peak ℓ_{peak} is investigated as the stability boundary at $n = 8457$ rpm is approached. In Fig. 5 the growth of this peak is illustrated: the peaks of the deterministic component slightly decrease, while peak of the stochastic component increases hyperbolically. Even if this peak is small it has a clearly visible effect on the time signal. It shows that the amplitude of the steady-state noise perturbation x_t is amplified near the border of the stable milling parameters due to the noise-induced resonance, since the characteristic damping of the milling process becomes 0 when losing stability, similarly as it has been illustrated in Appendix A.

To demonstrate the effect of the noise-induced resonance on the chatter-peak height ℓ_{peak}, the amplitude change is plotted for the spindle speed range $n \in [4800 \text{ rpm}, 8600 \text{ rpm}]$ in Fig. 6(c). To compare the above described quantities obtained with semidiscretization and MC simulations, the P2P of the stationary deterministic periodic first moment $x_{\text{p}}(t)$, the peak heights ℓ_{peak} and the mean and maximum values of the stationary standard deviation of the noise perturbation x_t are plotted in Fig. 6. Note that P2P of the stationary first moment in Fig. 6(b) do not show any particular behavior near the stability borders, only its magnitude grows at the resonant spindle speed $\Omega = \omega_{\text{n}}/Z$, as it is a well-known phenomenon [6,22,38]. However, the chatter-peak heights ℓ_{peak} in the Fourier spectrum of the stochastic perturbation x_t blow up near the stability borders as shown in Fig. 6(c). Furthermore, both the maximum and the mean of the stationary standard deviation $\text{StD}(x_t)$ in Fig. 6(d) blow up near the stability borders, due to noise-induced resonance, similarly to the peak height ℓ_{peak}. It can be observed, that only the maximum value shows an increase at the deterministic resonance, the mean standard deviation is insensitive to it. Note that the square root of the peaks ℓ_{peak} is shown for eyeballing purposes, and to allow the direct comparison with the standard deviations.

The results presented in this section show that by filtering the noisy components from the measured signal, important information is eliminated since, based on deterministic values, e.g., the averaged P2P values, the forthcoming chatter cannot be predicted and detected. Utilizing the stochastic effects, a model-based quantification of chatter prediction is possible, and the measurement difficulties in the chatter detection close to the stability boundary can be explained and predicted by the proposed stochastic model of milling.

3. Stochastic effects during chatter detection in milling

In this section it is experimentally investigated how the theoretical results in the previous Section 2 translate into practice. Namely, how well the stochastic milling model can describe the qualitative behavior of the real milling process. The stationary second moment of the measured displacements as well as the peak growth in the Fourier spectrum of the measured signal is investigated as the spindle speed Ω of the milling is varied.

For the measurements the same experimental setup is applied, as in [26] (see Fig. 7). During the measurements the milled workpiece is clamped onto a specially prepared flexure, which was designed to be flexible only in one direction, thus it can mimic the dynamics of a single-degree-of-freedom system. This measurement setup can replicate the dominant vibration mode of a thin walled workpiece. The milling tool is magnitudes of order stiffer than the flexible direction of this flexure, thus it can be considered rigid. The feed direction of the operation is chosen to be perpendicular to y (as shown in Fig. 7), leading to the same setup that's dynamics is described by Eq. (7) in Section 2. Note that in [26] it is thoroughly demonstrated that the deterministic part of this mechanical model is capable of capturing the stability properties, which is consistent with the results presented in Fig. 4, namely, the small noise intensity in the cutting force has negligible effect on the stability.

During the analysis of the vibrations, no external perturbations were applied on the system, only the vibrations of the workpiece caused by the milling force were measured by means of a piezoelectric accelerometer. To analyze the displacement signal, the measured acceleration is integrated in the frequency domain and an appropriate high-pass filter was used. Furthermore, from the measured signal only that section is used where the radial immersion, thus the entering φ_{en} and exiting φ_{ex} angles are constant, and the transient vibrations have decayed.

After the integration, the measured displacement y_t is decomposed into a deterministic $f_Z x_{\text{p}}(t)$ and into a stochastic $f_Z x_t$ component.

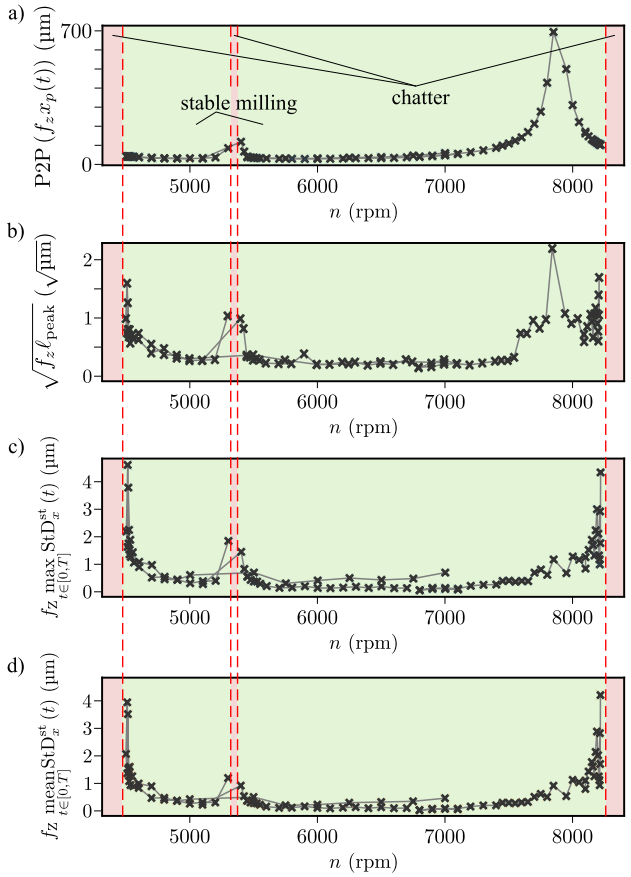

Fig. 8. Measured quantities during the milling operation. Panel a) shows the P2P values of the mean periodic solution, panel b) illustrates the behavior of the peak height $f_Z \ell_{\text{peak}}$ of the Fourier spectrum of the stochastic component $f_Z x_t$ while panel c) and d) shows the maximum and mean values of the standard deviation of the stochastic component of the vibrations, respectively. The lines connecting the crosses denote individual measurement series.

To obtain the deterministic component $f_Z x_p(t)$, the tooth passing frequency ω_Z has to be accurately determined, since the periodic averaging has to be conducted with respect to its period T_Z. In the ideal case the tooth passing frequency could be determined from the nominal spindle speed Ω of the tool as $\omega_Z = Z\Omega$. However, in practice this frequency is not accurate enough, since there is a small deviation (~ 0.1 %) between the prescribed Ω and the realized $\widetilde{\Omega}$ spindle speeds. The actual spindle speed $\widetilde{\Omega}$ is determined using the same approach as in [26]. Since the cutting force exciting the workpiece is a non-smooth function, the Fourier spectrum of the corresponding periodic forced vibrations contains the harmonics of the tooth passing frequency ω_Z and at its integer multiplies. The nominal spindle speed is used as an initial guess to initiate the calculation of the realized spindle speed $\widetilde{\Omega}$, which is determined by detecting the 50th higher harmonic of the tooth passing frequency ω_Z. With this approach, the realized spindle speed $\widetilde{\Omega}$ (and therefore the corresponding ω_Z) is obtained accurately enough to allow the calculation of the periodic solution $f_Z x_p(t)$ and the periodic standard deviation $\text{StD}(f_Z x_t)$ through periodic averaging and periodic standard deviation calculation, respectively, where the stochastic perturbation $f_Z x_t$ is obtained by

$$f_Z x_t = y_t - f_Z x_p(t). \tag{22}$$

The stochastic perturbation can be used to predict noise-induced resonance through the calculation of the maximum and mean of periodic standard deviation of $f_Z x_t$. Another approach to show the presence of the noise-induce resonance is to take the Fourier spectrum $|\widehat{x}_\omega|$ of the stochastic perturbation x_t and determine its maximum peak height ℓ_{peak} near $\omega = \omega_n$, where ω_n is the natural frequency of the workpiece-flexure composition. According to the theoretical results in Section 2, as the border of the stable parameter region is approached, the above described quantities increase hyperbolically.

The chatter detection strategy described above is applied to a case study similar to the theoretical model in Section 2: the axial depth of cut is fixed to $a_p = 2$mm, while the spindle speed is varied in the range $n \in [4500\ \text{rpm}, 8218\ \text{rpm}]$ with average steps of 100 rpm and near the stability borders with extremely small steps 2–5 rpm. The modal parameters, the cutting force characteristics are the same as in Section 2. The milling operations are conducted with a two-fluted Tivoly D16 Z2 L89/32 d16 VHM+HC P615 tool ($Z = 2$) with diameter $D = 16$ mm, helix angle $\beta = 30°$, while the feed per tooth was chosen as $f_Z = 0.1$ mm/tooth. Furthermore, these down-milling

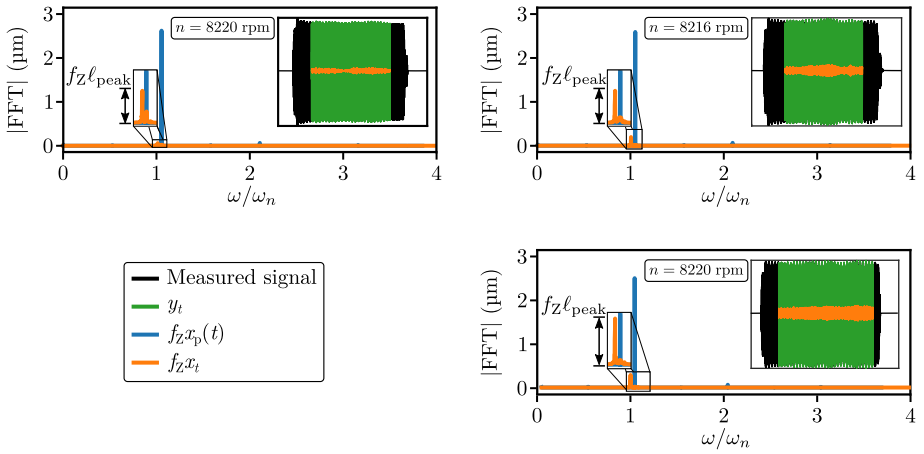

Fig. 9. Examples of the measured force signals and the corresponding Fourier transforms of the decomposed measured vibrations. The blue peaks denote the Fourier transforms of the periodic deterministic solution, while the orange peaks denote the Fourier transforms of the noise perturbation. For each Fourier transforms the measured displacement is given in green, the stochastic component is shown with the orange trajectory. The spindle speed Ω in each panel correspond to the nominal spindle speed.

tests were conducted along a straight path, with radial immersion $a_e = 2$ mm, which results in $\varphi_{en} \approx 138.6^\circ$ and $\varphi_{ex} = 180^\circ$. The length of the workpiece in the feed direction was 100 mm which resulted in approximately 1000 cutting cycles with the applied $f_Z = 0.1$ mm/tooth (that translated into 500 tool rotations, since $Z = 2$). The parameters of the calculations in Section 2 are chosen to be similar to these measurements to allow a direct qualitative comparison theoretical results obtained there. Note that the effect of the helix angle $\beta = 30^\circ$ is negligible due to the small axial immersion a_p.

The measurements were carried out on an NCT EmR-610Ms milling machine, where the workpiece was clamped onto the flexure. The vibration signals were acquired by B&K 4397 type acceleration sensor and the vibration data was collected with a NI-9234 Input Module in a NI cDAQ-9178 Chassis at 51200 Hz sampling rate.

In Fig. 8 some properties of the measured signal is shown, namely the peak-to-peak value $\mathrm{P2P}\big(f_Z x_p(t)\big)$ of the mean periodic displacement $f_Z x_p(t)$, the $f_Z \ell_{peak}$ of the FFT of stochastic signal $f_Z x_t$ and the maximum and mean values of the standard deviation $\mathrm{StD}(f_Z x_t)$, respectively. These properties of the measured signals show strong similarity to the theoretical results shown in Section 2. The peak-to-peak value $\mathrm{P2P}\big(f_Z x_p(t)\big)$ does not show any particular behavior near the stability borders and its magnitude grows at the resonant spindle speed $\Omega = \omega_n/Z$, which is expected based on the deterministic models.

However, in contrast to the theoretical results, there are increased $\mathrm{P2P}\big(f_Z x_p(t)\big)$ values around $5300-5500$ rpm, which corresponds to a flip bifurcation predicted by theoretical models at that spindle speed range [23]. A typical source of this phenomenon is the tool-runout that breaks the symmetry and the perfect time-periodicity of the cutting process [54]. Another typical reason for such inaccuracy is the slightly varying spindle speed, which can also raise new frequency components in the spectra. Furthermore, even a small variation of spindle speed makes it impossible to perfectly decompose the measured signal into a mean periodic and into a stochastic component.

The peak heights ℓ_{peak} in the Fourier spectrum of the stochastic component x_t blow up at all the stability borders as predicted by the theory. Discrepancies at the resonant spindle speed might be due to the above mentioned measurement problems, which cause a small portion of the deterministic component still being present in the stochastic component x_t, and this leads to the increase in the peak height ℓ_{peak} at the resonant spindle speeds. Note that this increase is only relatively large, since in absolute value it is only a $4-5\,\mu$m (compared to the mean's peak height which is $\sim 350\,\mu$m). Some examples for the growth of the $f_Z \ell_{peak}$ at the stability borders are shown in Fig. 9, where the measured signal and its FFT is presented. Furthermore, both the maximum and the mean of the stationary standard deviation $\mathrm{StD}(x_t)$ in Fig. 8(c)–(d) blow up at all the stability borders due to the noise-induced resonance, similarly to the peak height ℓ_{peak}.

As for the standard deviations, the difference between the maximum and the mean is only approximately a multiplier ($\sim 1.5\times$), but they show the same behavior, while the theoretical results predict a slight difference at the resonant spindle speed. This can be also the consequence of the varying spindle speed, since during the averaging, the effects causing the different behavior in the maximum and mean of the $\mathrm{StD}(f_Z x_t)$ are mitigated by this small variation of the spindle speed. Nonetheless, the standard deviation $\mathrm{StD}(f_Z x_t)$ is a good model based candidate for chatter indicator, since it does not produce a false positive or marginal uncertain measurement result and shows the same type of behavior near the stability borders, as predicted by the theory. However, the measurement of such a small standard deviation is challenging during a real practical scenario, due to the measurement is being overloaded by noise related to other sources, while the $f_Z \ell_{peak}$ can be still well tracked, thus the state-of-the-art approaches are based on this quantity.

This ℓ_{peak} is used intuitively by scientists and engineers, as a base value since decades. However, in this work a rigorous mathematical description provides an explanation on why a "chatter peak" appears in the stable domain during cutting experiments.

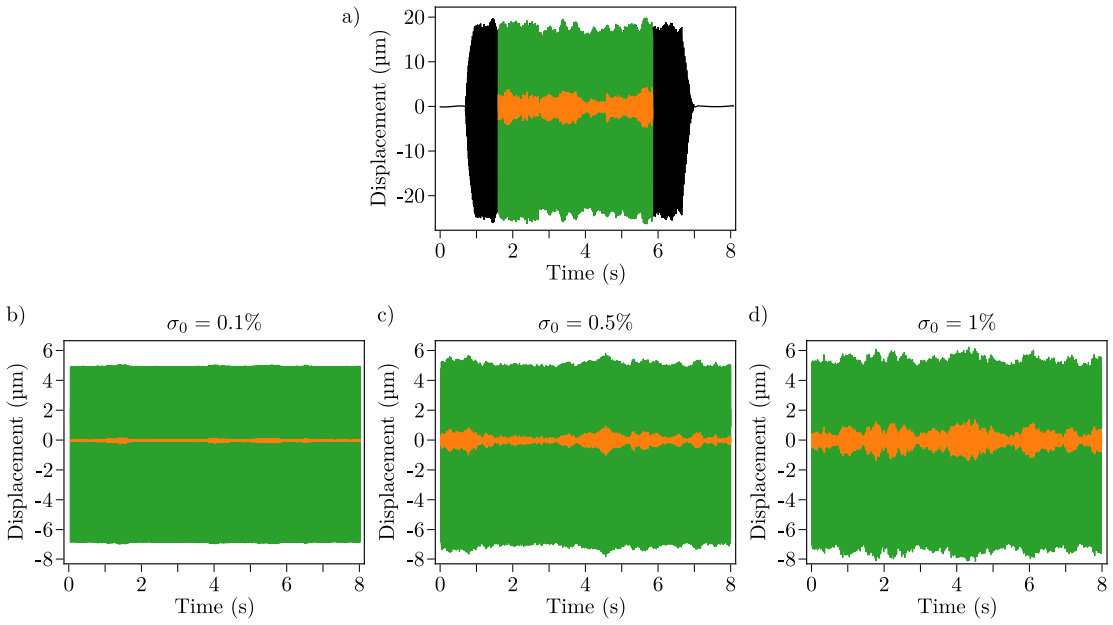

Fig. 10. Comparison of the a) measured signal at $n = 4600$ rpm with simulated signals b)–d) with parameters used in Section 2 at $n = 5100$ rpm (both spindle speed is in the domain of stable milling, and ~ 100 rpm from the stability border.

4. Conclusions and discussion

In this work, the noise-induced resonance in milling operations is investigated. The theoretical analysis explain the presence of the so-called chatter peaks in the spectra of the measured vibrations signals under stable machining conditions. The steady-state stochastic component of the machine tool vibrations are shown to grow hyperbolically as the stability boundaries are approached. The results are supported by an experimental case study.

First, the theoretical explanation of the phenomenon is given with the help of the stochastic single-degree-of-freedom model of milling, namely, that it is caused by the stochastic noise-induced resonance. It was shown that the influence of the fluctuating cutting force on the stability of milling is negligible. However, as the border of the stable cutting parameters is approached the effects of the noise in the stationary solution are magnified, while in the steady-state deterministic periodic solution $x_p(t)$ no particular behavior can be observed. This increase can be observed in the Fourier transformed vibration signals: a peak emerges at the chatter frequency near the natural frequency ω_n of the mechanical system. Similarly, the steady-state $\mathbb{E}(x_t^2)$ of the stochastic perturbation x_t grows hyperbolically near the critical parameter values. This shows that the vibrations are deviating from the deterministic steady-state solution $x_p(t)$ in an increasing manner as the characteristic damping of the system decreases to zero, and eventually the unstable chatter vibrations occur.

These indicate that even seemingly negligible noise fluctuations in the cutting force can cause a resonance effect near the stability borders, leading to difficulties in chatter detection, or it can even cause the transition to chatter in the unsafe (bistable) zones near the stability borders [16,36]. Moreover, this behavior indicates that by filtering the noisy components of the vibration signals important information is eliminated, and utilizing only the attributes of the signal based on deterministic phenomena, the forthcoming chatter cannot be predicted or detected reliably.

To validate the theoretical results a detailed series of milling tests were performed. The results obtained during the measurements showed good agreement with the theoretical predictions, however, there were some minor qualitative differences. First, the measured chatter peaks in the FFT of the measured stochastic perturbation process x_t show an increase in case of the resonant spindle speed $\Omega \approx \omega_n/Z$. Secondly, the maximum and the time average of the periodic steady-state standard deviation do not differ from each other qualitatively for the measurements, while the theoretical calculations predict an increase in the maximum standard deviation near the resonant spindle speed. These differences can be attributed to the slight (1–2 rpm) fluctuations in the spindle speed, since the method relies on partitioning the measured signal into a steady-state deterministic periodic solution $x_p(t)$ and into a stationary stochastic component x_t. If the periodic deterministic component is not perfectly determined, then the calculation of the other periodic quantities also lead to inaccurate results. In case of the chatter peak height ℓ_{peak} the steady-state deterministic component is not completely removed from the stochastic perturbation (even if only a rather small portion is the remainder), thus the unpredicted increase is shown in the measurement results. For the periodic second moment, the periodicity is blurred by this effect.

As a summary, the stochastic analysis of the milling process can provide a qualitative description of the noise component in the stable domain, which can be utilized to detect the emerging chatter. Furthermore, near the stability borders, due to the noise-induced resonance, the theoretical model is really sensitive [10,28] to slight changes, e.g., varying spindle speed, tool run-out, helical edge

geometry and the fly-overs even at small-amplitude vibrations. Moreover, for a better quantitative comparison, the intensity of the noise process as well as the other parameter of the model can be tuned, however, it is not trivial how the stochastic component of the cutting force should be adjusted. Namely, the intensity σ_0 should be decreased in the theoretical model (7) to fit the calculated peak values ℓ_{peak} and standard deviations $\text{StD}(f_Z x_t)$ to their measured counterparts, while based on the visual inspection of the time signals presented in Fig. 10 this intensity σ_0 should be increased, relative to the measured intensity presented in [19].

To conclude, in this paper the stochastic single-degree-of-freedom model of milling is investigated, where the high-frequency fluctuations in the cutting force is substituted by a Gaussian white noise process. With the help of the stochastic model of milling the formulation of a chatter peak in the FFT of the signal in the stable machining parameter domains are explained as the manifestation of the noise-induced resonance near the stability borders. It is shown, that near the critical machining parameters both the height of the so-called chatter peak in the FFT and the steady-state second moment of the simulated and measured vibrations grow hyperbolically. The theoretical findings are validated through a series of milling experiments, which produce results that are in good agreement with the predicted behavior. Utilizing the results of this paper, more reliable chatter detection methods can be constructed, where the stable, the resonant and the unstable vibrations are distinguished based on physical models and quantities.

CRediT authorship contribution statement

Henrik T Sykora: Conceptualization, Methodology, Software, Formal analysis, Visualization, Writing - original draft. **David Hajdu:** Investigation, Writing - review & editing. **Zoltan Dombovari:** Writing - review & editing, Funding acquisition. **Daniel Bachrathy:** Conceptualization, Supervision, Writing - review & editing, Funding acquisition.

Declaration of Competing Interest

The authors declare that they have no known competing financial interests or personal relationships that could have appeared to influence the work reported in this paper.

Acknowledgements

This work was supported by the Hungarian Scientific Research Fund (OTKA FK-124462). The research reported in this paper and carried out at BME has been supported by the Hungarian National Research, Development and Innovation Office (NKFI-K-132477 and NKFI-KKP-133846) and by the NRDI Fund (TKP2020 IES, Grant No. BME-IE-MIFM and TKP2020 NC, Grant No. BME-NC) based on the charter of bolster issued by the NRDI Office under the auspices of the Ministry for Innovation and Technology.

Appendix A. Noise-induced resonance

Since the white noise process Γ_t has a constant power spectral density [5,39], it has the potential to cause a resonance effect. To demonstrate this, consider the dimensionless equation of motion of the single-degree-of-freedom linear oscillator subjected to white noise excitation:

$$\dot{x}_t + 2\zeta\dot{x}_t + x_t = \sigma_0\Gamma_t, \tag{23}$$

where ζ is the damping coefficient. Eq. (23) and has the first-order incremental form

$$\mathrm{d}\mathbf{x}_t = \mathbf{A}\mathbf{x}_t\mathrm{d}t + \boldsymbol{\sigma}\mathrm{d}W_t, \quad \mathbf{x}_t = \begin{pmatrix} x_t \\ \dot{x}_t \end{pmatrix}, \quad \mathbf{A} = \begin{pmatrix} 0 & 1 \\ -1 & -2\zeta \end{pmatrix}, \quad \boldsymbol{\sigma} = \begin{pmatrix} 0 \\ \sigma_0 \end{pmatrix}. \tag{24}$$

The solution of (24) can be written [5] as

$$\mathbf{x}_t = e^{\mathbf{A}t}\mathbf{x}_0 + \int_0^t e^{\mathbf{A}(t-\widehat{t})}\boldsymbol{\sigma}\mathrm{d}W_{\widehat{t}}. \tag{25}$$

In case of a stable system with moderate damping ($0 < \zeta \ll 1$) the stationary moments are

$$\lim_{t\to\infty}\mathbb{E}(\mathbf{x}_t) = \mathbf{0}, \qquad \lim_{t\to\infty}\mathbb{E}\left(\mathbf{x}_t\mathbf{x}_t^\top\right) = \begin{pmatrix} \frac{\sigma_0^2}{4\zeta} & 0 \\ 0 & \frac{\sigma_0^2}{4\zeta} \end{pmatrix}. \tag{26}$$

Note that in case of small damping, even if the average tends to zero, there can persist a significant noisy motion.

This consequence can be derived using a different approach. The oscillator (24) is often characterised by using the absolute value of the frequency response function (resonance curve):

$$R(\omega) = \frac{1}{\sqrt{(1-\omega^2)^2 + 4\zeta^2\omega^2}}. \tag{27}$$

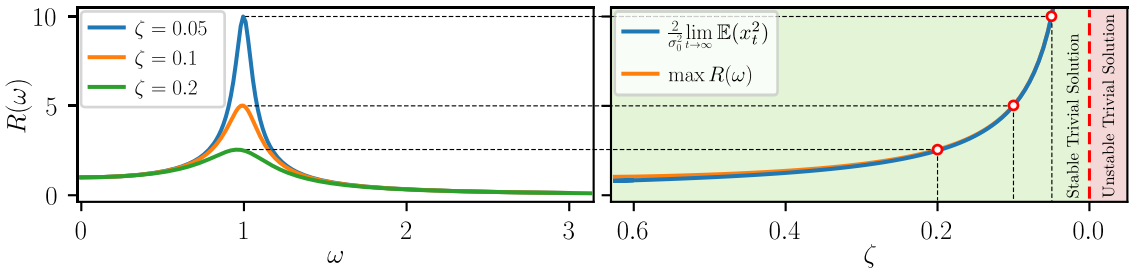

Fig. 11. Resonance curves and the comparison of the stationary second moment and the maximum value of resonance curve for system (24).

The resonance curve $R(\omega)$ describes the amplification rate of the mechanical system (24) for each frequency ω for a given force excitation. In case of a deterministic harmonic excitation resonance occurs if the excitation frequency matches the natural frequency of the system.

Since the white noise Γ_t excites all the frequencies with the same magnitude the resonant excitation is unavoidable. The worst case, the maximum of the amplification described by the maximum of the resonance curve $R(\omega)$ is a good measure to investigate the maximal response of the system (24) given by

$$\max_{\omega} R(\omega) = \frac{1}{2\zeta\sqrt{1-\zeta^2}} \tag{28}$$

at $\omega = \sqrt{1-2\zeta^2}$, or for $0 < \zeta \ll 1$

$$\max_{\omega} R(\omega) \approx \frac{1}{2\zeta} \tag{29}$$

at $\omega \approx 1$, thus the noise is inversely proportional to the damping ζ.

Comparing the stationary second moment in (26) and the maximum amplification near small ζ values in (29) it can be seen, that the two quantity increase hyperbolically as approaching the critical damping value $\zeta = 0$ (see Fig. 11). This observation can be utilized, to use the stationary second moment to qualitatively describe systems near critical parameters. In case of bifurcation analysis, when the system changes from stable to unstable, e.g., in model (24) the bifurcation parameter ζ goes through zero, the second moment of the vibration tends to infinity even before reaching the unstable zone. Note that in case of more complex models (e.g., a non-smooth, nonlinear model of turning in [15]) the effect of noise-induced resonance is saturated near the bifurcation point of the trivial solution, thus the linear model is gives only good approximation for smaller amplitude vibrations.

References

[1] Y. Altintas, Manufacturing Automation: Metal Cutting Mechanics, Machine Tool Vibrations, and CNC Design, 2 edition,, Cambridge University Press, 2012.
[2] Y. Altintas, A. Ber, Manufacturing Automation: Metal Cutting Mechanics, Machine Tool Vibrations, and CNC Design, vol. 54, 2001.
[3] Y. Altintas, P.K. Chan, In-process detection and suppression of chatter in milling, International Journal of Machine Tools and Manufacture 32 (3) (1992) 329–347.
[4] Y. Altintas, P.K. Chan, In-process detection and suppression of chatter in milling, International Journal of Machine Tools and Manufacture 32 (3) (1992) 329–347.
[5] L. Arnold, Stochastic Differential Equations: Theory and Applications, R. Oldenbourg Verlag, Munich, 1973.
[6] D. Bachrathy, T. Insperger, G. Stépán, Surface properties of the machined workpiece for helical mills, Machining Science and Technology 13 (2) (May 2009) 227–245.
[7] I. Bediaga, I. Egaña, J. Munoa, M. Zatarain, L. Lacalle, Chatter avoidance method for milling process based on sinusoidal spindle speed variation method: simulation and experimental results, in: 10th CIRP International Workshop on Modeling of Machining Operations, Reggio Calabria, Italy, Aug. 2007.
[8] S. Berezvai, T. Molnar, D. Bachrathy, G. Stepan, Experimental investigation of the shear angle variation during orthogonal cutting, Materials Today: Proceedings 5 (2018) 26495–26500.
[9] S. Berezvai, T.G. Molnar, A. Kossa, D. Bachrathy, G. Stepan, Numerical and experimental investigation of contact length during orthogonal cutting, Materials Today: Proceedings 12 (2019) 329–334.
[10] E. Buckwar, R. Kuske, B. L'esperance, T. Soo, Noise-sensitivity in machine tool vibrations, International Journal of Bifurcation and Chaos 16 (08) (2006) 2407–2416.
[11] E. Budak, Y. Altintas, Analytical prediction of chatter stability in milling – Part I: General formulation, Journal of Dynamic Systems, Measurement, and Control 120 (1) (1998) 22–30.
[12] E. Budak, Y. Altintas, E.J.A. Armarego, Prediction of milling force coefficients from orthogonal cutting data, Journal of Manufacturing Science and Engineering 118 (2) (1996) 216–224.
[13] K. Cheminski, D. Hömberg, O. Rott, On a thermomechanical milling model, Nonlinear Analysis: Real World Applications 12 (1) (2011) 615–632.
[14] T. Delio, J. Tlusty, S. Smith, Use of audio signals for chatter detection and control, Journal of Engineering for Industry 114 (2) (1992) 146–157.
[15] Z. Dombovari, D.A. Barton, R.E. Wilson, G. Stepan, On the global dynamics of chatter in the orthogonal cutting model, International Journal of Non-Linear Mechanics 46 (1) (2011) 330–338.
[16] Z. Dombovari, A. Iglesias, T. Molnar, G. Habib, J. Munoa, R. Kuske, G. Stépán, Experimental observations on unsafe zones in milling processes, Philosophical Transactions of the Royal Society A: Mathematical, Physical and Engineering Sciences 377 (2153) (2019).

[17] R. Du, M. Elbestawi, B. Ullagaddi, Chatter detection in milling based on the probability distribution of cutting force signal, Mechanical Systems and Signal Processing 6 (4) (1992) 345–362.
[18] R. Faassen, E. Doppenberg, N. Wouw, van de, J. Oosterling, H. Nijmeijer, Online detection of the onset and occurrence of machine tool chatter in the milling process, in: CIRP 2nd International Conference on High Performance Cutting, pages paper-no. 23, 2006.
[19] G. Fodor, H.T. Sykora, D. Bachrathy, Stochastic modeling of the cutting force in turning processes, Accepted for publication: The International Journal of Advanced Manufacturing Technology (2020).
[20] G. Gyebrószki, D. Bachrathy, G. Csernák, G. Stépán, Stability of turning processes for periodic chip formation, Advances in Manufacturing 6 (3) (2018) 345–353.
[21] D. Hajdu, T. Insperger, D. Bachrathy, G. Stepan, Prediction of robust stability boundaries for milling operations with extended multi-frequency solution and structured singular values, Journal of Manufacturing Processes 30 (2017) 281–289.
[22] T. Insperger, J. Gradišek, M. Kalveram, G. Stépán, K. Winert, E. Govekar, Machine tool chatter and surface location error in milling processes, Journal of Manufacturing Science and Engineering 128 (4) (2006) 913–920.
[23] T. Insperger, J. Munoa, M.a. Zatarain, G. Peigné, Unstable islands in the stability chart of milling processes due to the helix angle, in: CIRP 2nd International Conference on High Performance Cutting, Vancouver, Canada, 2006, pp. 12–13.
[24] T. Insperger, G. Stepan, Semi-Discretization for Time-Delay Systems: Stability and Engineering Applications. Applied Mathematical Sciences, Springer, New York, 2011.
[25] F.A. Khasawneh, E. Munch, Chatter detection in turning using persistent homology, Mechanical Systems and Signal Processing 70–71 (2016) 527–541.
[26] A.K. Kiss, D. Hajdu, D. Bachrathy, G. Stepan, Operational stability prediction in milling based on impact tests, Mechanical Systems and Signal Processing 103 (2018) 327–339.
[27] E. Kuljanic, M. Sortino, G. Totis, Multisensor approaches for chatter detection in milling, Journal of Sound and Vibration 312 (4–5) (2008) 672–693.
[28] R. Kuske, Competition of noise sources in systems with delay: the role of multiple time scales, Journal of Vibration and Control 16 (7–8) (2010) 983–1003.
[29] D. Lehotzky, T. Insperger, F. Khasawneh, G. Stepan, Spectral element method for stability analysis of milling processes with discontinuous time-periodicity, The International Journal of Advanced Manufacturing Technology 89 (9–12) (2017) 2503–2514.
[30] K. Li, S. He, B. Li, H. Liu, X. Mao, C. Shi, A novel online chatter detection method in milling process based on multiscale entropy and gradient tree boosting, Mechanical Systems and Signal Processing 135 (2020), 106385.
[31] Y. Liao, Y. Young, A new on-line spindle speed regulation strategy for chatter control, International Journal of Machine Tools and Manufacture 36 (5) (1996) 651–660.
[32] J. Lipski, G. Litak, R. Rusinek, K. Szabelski, A. Teter, J. Warmi'nski, K. Zaleski, Surface quality of a work materials influence on the vibrations of the cutting process, Journal of Sound and Vibration 252 (4) (2002) 729–737.
[33] C. Liu, L. Zhu, C. Ni, Chatter detection in milling process based on VMD and energy entropy, Mechanical Systems and Signal Processing 105 (2018) 169–182.
[34] H. Liu, Q. Bo, H. Zhang, Y. Wang, Analysis of q-factor's identification ability for thin-walled part flank and mirror milling chatter, The International Journal of Advanced Manufacturing Technology 99 (5–8) (2018) 1673–1686.
[35] B.P. Mann, K.A. Young, An empirical approach for delayed oscillator stability and parametric identification, Proceedings of the Royal Society A: Mathematical, Physical and Engineering Sciences 462 (2071) (2006) 2145–2160.
[36] T.G. Molnár, T. Insperger, S.J. Hogan, G. Stépán, Estimation of the bistable zone for machining operations for the case of a distributed cutting-force model, Journal of Computational and Nonlinear Dynamics 11 (5) (2016).
[37] T.G. Molnar, T. Insperger, G. Stepan, Closed-form estimations of the bistable region in metal cutting via the method of averaging, International Journal of Non-Linear Mechanics 112 (49–56) (2019).
[38] D. Montgomery, Y. Altintas, Mechanism of cutting force and surface generation in dynamic milling, Journal of Engineering for Industry 113 (2) (1991) 160–168.
[39] B. Øksendal, Stochastic Differential Equations, Springer, Berlin, Heidelberg, 2003.
[40] Z. Palmai, G. Csernak, Chip formation as an oscillator during the turning process, Journal of Sound and Vibration 326 (2009) 809–820.
[41] J. Prohaszka, J. Dobranszky, The role of an anisotropy of the elastic moduli in the determination of the elastic limit value, Materials Science Forum – MATER SCI FORUM 414–415 (2003) 311–316.
[42] J. Prohaszka, J. Dobranszky, J. Nyiró, M. Horvath, A. Mamalis, Modifications of surface integrity during the cutting of copper, Materials and Manufacturing Processes 19 (2004) 1025–1039.
[43] J. Prohaszka, A.G. Mamalis, M. Horvath, J. Nyiro, J. Dobranszky, Effect of microstructure on the mirror-like surface quality of fcc and bcc metals, Materials and Manufacturing Processes 21 (8) (2006) 810–818.
[44] G. Quintana, J. Ciurana, Chatter in machining processes: A review, International Journal of Machine Tools and Manufacture 51 (5) (2011) 363–376.
[45] C. Rackauckas, Q. Nie, Adaptive methods for stochastic differential equations via natural embeddings and rejection sampling with memory, Discrete & Continuous Dynamical Systems - B 22 (7) (2017) 2731–2761.
[46] R. Rusinek, P. Lajmert, Chatter detection in milling of carbon fiber-reinforced composites by improved hilbert–huang transform and recurrence quantification analysis, Materials 13 (18) (2020) 4105.
[47] M. Shiraishi, Scope of in-process measurement, monitoring and control techniques in machining processes—part 3: In-process techniques for cutting processes and machine tools, Precision Engineering 11 (1) (1989) 39–47.
[48] H.T. Sykora, Julia package: Stochasticsemidiscretizationmethod.jl, v0.3.3. https://github.com/HTSykora/StochasticSemiDiscretizationMethod.jl, 2021-03-08.
[49] H.T. Sykora, D. Bachrathy, Stochastic semidiscretization method: Second moment stability analysis of linear stochastic periodic dynamical systems with delays, Applied Mathematical Modelling 88 (2020) 933–950.
[50] H.T. Sykora, D. Bachrathy, G. Stepan, Gaussian noise process as cutting force model for turning, Procedia CIRP 77 (2018) 94–97 (8th CIRP Conference on High Performance Cutting (HPC 2018)).
[51] H.T. Sykora, D. Bachrathy, G. Stepan, Stochastic semi-discretization for linear stochastic delay differential equations, International Journal for Numerical Methods in Engineering 119 (9) (2019) 879–898.
[52] J. Tlusty, L. Spacek, Self-excited vibrations on machine tools, Nakl. CSAV, Prague. in Czech., 1954.
[53] S.A. Tobias, Machine-tool Vibration, Blackie, Glasgow, 1965.
[54] G. Totis, T. Insperger, M. Sortino, G. Stépán, Symmetry breaking in milling dynamics, International Journal of Machine Tools and Manufacture 139 (2019) 37–59.
[55] G. Totis, M. Sortino, Polynomial chaos-kriging approaches for an efficient probabilistic chatter prediction in milling, International Journal of Machine Tools and Manufacture 157 (2020), 103610.
[56] S. Wan, X. Li, Y. Yin, J. Hong, Milling chatter detection by multi-feature fusion and adaboost-SVM, Mechanical Systems and Signal Processing 156 (2021), 107671.
[57] M. Wiercigroch, E. Budak, Sources of nonlinearities, chatter generation and suppression in metal cutting, Philosophical Transactions of the Royal Society of London. Series A: Mathematical, Physical and Engineering Sciences 359 (1781) (2001) 663–693.